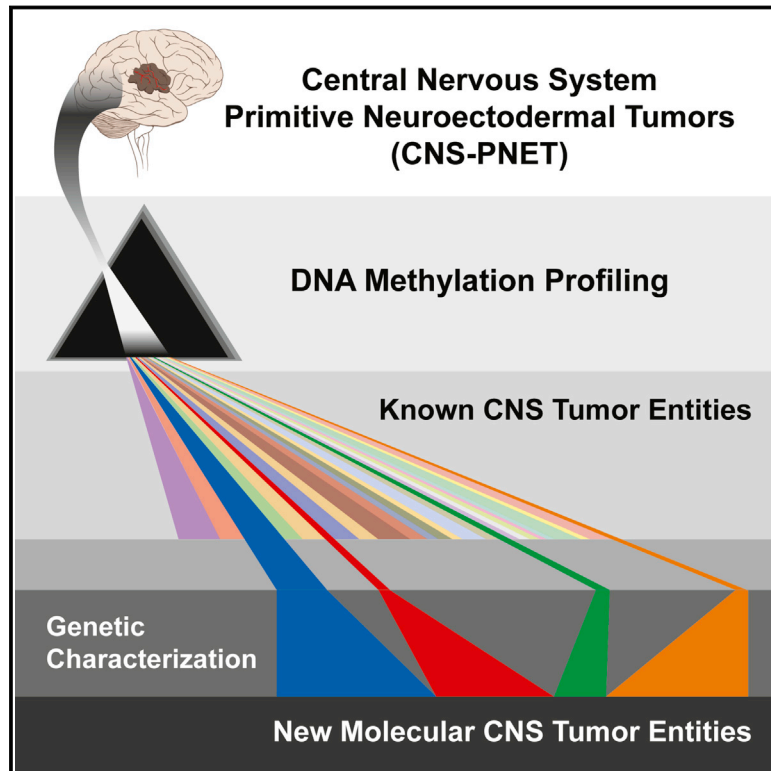# New Brain Tumor Entities Emerge from Molecular Classification of CNS-PNETs

Graphical Abstract

Authors

Dominik Sturm, Brent A. Orr,
Umut H. Toprak, ..., David W. Ellison,
Andrey Korshunov, Marcel Kool

Correspondence

m.kool@dkfz.de

In Brief

Highly malignant primitive neuroectodermal tumors of the CNS (CNS-PNETs) have been challenging to diagnose and distinguish from other kinds of brain tumors, but molecular profiling now reveals that these cancers can be readily classified into some known tumor types and four new entities with distinct histopathological and clinical features, paving the way for meaningful clinical trials.

Highlights

- A large fraction of CNS-PNETs can be re-classified into other CNS tumor entities

- Four new CNS tumor entities emerge from the remaining fraction of CNS-PNETs

- Each new entity is associated with distinct histological and clinical features

- Each new entity is characterized by a defining recurrent genetic alteration

Accession Numbers

GSE73038
GSE73801

New Brain Tumor Entities Emerge from Molecular Classification of CNS-PNETs

Dominik Sturm,[1,2,3,89] Brent A. Orr,[4,89] Umut H. Toprak,[2,5,89] Volker Hovestadt,[2,6,89] David T.W. Jones,[1,2] David Capper,[2,7,8] Martin Sill,[2,9] Ivo Buchhalter,[2,5] Paul A. Northcott,[1,2] Irina Leis,[7] Marina Ryzhova,[10] Christian Koelsche,[2,7,8] Elke Pfaff,[1,2,3] Sariah J. Allen,[4] Gnanaprakash Balasubramanian,[2,11] Barbara C. Worst,[1,2,3] Kristian W. Pajtler,[1,2] Sebastian Brabetz,[1,2] Pascal D. Johann,[1,2,3] Felix Sahm,[2,7,8] Jüri Reimand,[12,13] Alan Mackay,[14] Diana M. Carvalho,[14] Marc Remke,[15] Joanna J. Phillips,[16,17,18] Arie Perry,[16,17,18] Cynthia Cowdrey,[16] Rachid Drissi,[19] Maryam Fouladi,[19] Felice Giangaspero,[20,21] Maria Łastowska,[22] Wiesława Grajkowska,[22] Wolfram Scheurlen,[23] Torsten Pietsch,[24] Christian Hagel,[25] Johannes Gojo,[26,27] Daniela Lötsch,[27] Walter Berger,[27] Irene Slavc,[26] Christine Haberler,[28] Anne Jouvet,[29,30] Stefan Holm,[31] Silvia Hofer,[32] Marco Prinz,[33,34] Catherine Keohane,[35] Iris Fried,[36] Christian Mawrin,[37] David Scheie,[38] Bret C. Mobley,[39] Matthew J. Schniederjan,[40] Mariarita Santi,[41] Anna M. Buccoliero,[42] Sonika Dahiya,[43] Christof M. Kramm,[44] André O. von Bueren,[44] Katja von Hoff,[45] Stefan Rutkowski,[45] Christel Herold-Mende,[46] Michael C. Frühwald,[47] Till Milde,[2,3,48] Martin Hasselblatt,[49] Pieter Wesseling,[50,51] Jochen Rößler,[52] Ulrich Schüller,[53,54] Martin Ebinger,[55,71] Jens Schittenhelm,[56,71] Stephan Frank,[57] Rainer Grobholz,[58] Istvan Vajtai,[59] Volkmar Hans,[60] Reinhard Schneppenheim,[45] Karel Zitterbart,[61] V. Peter Collins,[62] Eleonora Aronica,[63] Pascale Varlet,[64] Stephanie Puget,[65] Christelle Dufour,[66] Jacques Grill,[66] Dominique Figarella-Branger,[67] Marietta Wolter,[68,69] Martin U. Schuhmann,[70,71] Tarek Shalaby,[72] Michael Grotzer,[72] Timothy van Meter,[73] Camelia-Maria Monoranu,[74,75] Jörg Felsberg,[68,69] Guido Reifenberger,[68,69] Matija Snuderl,[76] Lynn Ann Forrester,[77] Jan Koster,[78] Rogier Versteeg,[78] Richard Volckmann,[78] Peter van Sluis,[78] Stephan Wolf,[2,79] Tom Mikkelsen,[80] Amar Gajjar,[81] Kenneth Aldape,[82] Andrew S. Moore,[83,84] Michael D. Taylor,[15] Chris Jones,[14] Nada Jabado,[85] Matthias A. Karajannis,[86] Roland Eils,[2,5,87,88] Matthias Schlesner,[2,5] Peter Lichter,[2,6,88] Andreas von Deimling,[2,7,8] Stefan M. Pfister,[1,2,3] David W. Ellison,[4,90] Andrey Korshunov,[2,7,8,90] and Marcel Kool[1,2,90,*]

[1]Division of Pediatric Neurooncology, German Cancer Research Center (DKFZ) Heidelberg, 69120 Heidelberg, Germany
[2]German Cancer Consortium (DKTK) Core Center Heidelberg, 69120 Heidelberg, Germany
[3]Department of Pediatric Oncology, Hematology, & Immunology, Heidelberg University Hospital, 69120 Heidelberg, Germany
[4]Department of Pathology, St. Jude Children's Research Hospital, Memphis, TN 38105-3678, USA
[5]Division of Theoretical Bioinformatics, German Cancer Research Center (DKFZ) Heidelberg, 69120 Heidelberg, Germany
[6]Division of Molecular Genetics, German Cancer Research Center (DKFZ) Heidelberg, 69120 Heidelberg, Germany
[7]Department of Neuropathology, Heidelberg University Hospital, 69120 Heidelberg, Germany
[8]Clinical Cooperation Unit Neuropathology, German Cancer Research Center (DKFZ), 69120 Heidelberg, Germany
[9]Division of Biostatistics, German Cancer Research Center (DKFZ) Heidelberg , 69120 Heidelberg, Germany
[10]NN Burdenko Neurosurgical Institute, Moscow 125047, Russia
[11]Division of Applied Bioinformatics, German Cancer Research Center (DKFZ) Heidelberg, 69120 Heidelberg, Germany
[12]Ontario Institute for Cancer Research, Toronto, ON M5G 0A3, Canada
[13]Department of Medical Biophysics, University of Toronto, Toronto, ON M5G 1L7, Canada

SUMMARY

Primitive neuroectodermal tumors of the central nervous system (CNS-PNETs) are highly aggressive, poorly differentiated embryonal tumors occurring predominantly in young children but also affecting adolescents and adults. Herein, we demonstrate that a significant proportion of institutionally diagnosed CNS-PNETs display molecular profiles indistinguishable from those of various other well-defined CNS tumor entities, facilitating diagnosis and appropriate therapy for patients with these tumors. From the remaining fraction of CNS-PNETs, we identify four new CNS tumor entities, each associated with a recurrent genetic alteration and distinct histopathological and clinical features. These new molecular entities, designated "CNS neuroblastoma with *FOXR2* activation (CNS NB-*FOXR2*)," "CNS Ewing sarcoma family tumor with *CIC* alteration (CNS EFT-*CIC*)," "CNS high-grade neuroepithelial tumor with *MN1* alteration (CNS HGNET-*MN1*)," and "CNS high-grade neuroepithelial tumor with *BCOR* alteration (CNS HGNET-*BCOR*)," will enable meaningful clinical trials and the development of therapeutic strategies for patients affected by poorly differentiated CNS tumors.

INTRODUCTION

The CNS comprises many different pluripotent and differentiated cell types that vary greatly in abundance during human lifespan. This is reflected by a broad diversity of CNS tumor entities, some

[14]Division of Molecular Pathology, the Institute of Cancer Research, London SW7 3RP, UK

[15]Program in Developmental and Stem Cell Biology, Division of Neurosurgery, Arthur and Sonia Labatt Brain Tumour Research Centre, Hospital for Sick Children, University of Toronto, Toronto, ON M4N 1X8, Canada

[16]Brain Tumor Research Center, University of California, San Francisco, San Francisco, CA 94158-9001, USA

[17]Neuropathology, Department of Pathology, University of California, San Francisco, San Francisco, CA 94143-0102, USA

[18]Department of Neurological Surgery, University of California, San Francisco, San Francisco, CA 94143-0112, USA

[19]Division of Oncology, Cincinnati Children's Hospital Medical Center, Cincinnati, OH 45229, USA

[20]Department of Radiological, Oncological and Anatomic-Pathological Sciences, Sapienza University of Rome, 00185 Rome, Italy

[21]IRCCS Neuromed, 86077 Pozzilli, Molise, Italy

[22]Department of Pathology, Children's Memorial Health Institute, 04-730 Warsaw, Poland

[23]Cnopf'sche Kinderklinik, Nürnberg Children's Hospital, 90419 Nürnberg, Germany

[24]Department of Neuropathology, University of Bonn Medical School, 53105 Bonn, Germany

[25]Institute of Neuropathology, University Medical Center Hamburg-Eppendorf, 20246 Hamburg, Germany

[26]Department of Pediatrics and Adolescent Medicine, Medical University of Vienna, 1090 Vienna, Austria

[27]Department of Medicine I, Institute of Cancer Research and Comprehensive Cancer Center, Medical University of Vienna, 1090 Vienna, Austria

[28]Institute of Neurology, Medical University of Vienna, 1097 Vienna, Austria

[29]Neuro-Oncology and Neuro-Inflammation Team, Inserm U1028, CNRS UMR 5292, University Lyon-1, Neuroscience Center, 69000 Lyon, France

[30]Centre de Pathologie et de Neuropathologie Est, Hospices Civils de Lyon, 69003 Lyon, France

[31]Department of Women's and Children's Health (KBH), Karolinska Institutet, 171 77 Stockholm, Sweden

[32]Department of Oncology, Luzerner Kantonsspital, 6000 Luzern 16, Switzerland

[33]Institute of Neuropathology, University of Freiburg, 79106 Freiburg, Germany

[34]BIOSS Centre for Biological Signalling Studies, University of Freiburg, 79106 Freiburg, Germany

[35]Department of Pathology, University College Cork and Cork University Hospital Wilton, Cork T12 YN60, Ireland

[36]Department of Pediatric Hematology and Oncology, Hadassah Medical Center, Jerusalem 91120, Israel

[37]Institute of Neuropathology, University Hospital, Otto-von-Guericke University, 39120 Magdeburg, Germany

[38]Department of Pathology, Copenhagen University Hospital, 2100 København Ø, Denmark

[39]Department of Pathology, Microbiology, and Immunology, Vanderbilt University Medical Center, Nashville, TN 37232, USA

[40]Department of Pathology and Laboratory Administration, Children's Healthcare of Atlanta, Atlanta, GA 30322, USA

[41]Department of Pathology, Children's Hospital of Philadelphia, Philadelphia, PA 19104, USA

[42]Pathology Unit, Anna Meyer Children's University Hospital, 50141 Florence, Italy

[43]Department of Pathology and Immunology, Washington University, St. Louis, MO 63110, USA

[44]Division of Pediatric Hematology and Oncology, Department of Child and Adolescent Health, University Medical Center Göttingen, 37075 Göttingen, Germany

[45]Department of Pediatric Haematology and Oncology, University Medical Center Hamburg-Eppendorf, 20246 Hamburg, Germany

[46]Department of Neurosurgery, Heidelberg University Hospital, 69120 Heidelberg, Germany

[47]Pediatric Hospital, Klinikum Augsburg, 86156 Augsburg, Germany

[48]Clinical Cooperation Unit Pediatric Oncology, German Cancer Research Center (DKFZ) Heidelberg, 69120 Heidelberg, Germany

[49]Institute of Neuropathology, University Hospital Münster, 48149 Münster, Germany

[50]Department of Pathology, VU University Medical Center Amsterdam, 1008 MB Amsterdam, the Netherlands

[51]Department of Pathology, Radboud University Nijmegen Medical Center, 6525 GA Nijmegen, the Netherlands

[52]Department of Pediatric Hematology/Oncology, Center of Pediatrics and Adolescent Medicine, University Medical Center Freiburg, 79106 Freiburg, Germany

[53]Department of Neuropathology, Ludwig-Maximilians-University, 81377 Munich, Germany

[54]German Cancer Consortium (DKTK) Partner Site Munich, 81377 Munich, Germany

of which are relatively common, whereas others develop rarely, and many of them occur at defined ages. Primitive neuroectodermal tumors of the CNS (CNS-PNETs) are highly malignant neoplasms that predominantly affect children but may also arise in adolescents and adults. Histologically, CNS-PNETs are characterized by small, poorly differentiated or undifferentiated embryonal cells with a propensity for both glial and neuronal differentiation (Louis et al., 2007), but the neuropathological diagnosis is challenging due to a lack of defining molecular markers and histological overlap with other high-grade neuroepithelial tumors. The original concept related medulloblastoma (i.e., PNET of the cerebellum) to embryonal tumors of the cerebrum (supra-

tentorial PNET) (Rorke, 1983), but issues with the clinicopathological utility of classifying non-cerebellar CNS-PNETs have generated significant controversy over decades (Rorke et al., 1997). This resulted in considerable uncertainty regarding accurate diagnosis and optimal treatment for affected patients (Jakacki et al., 2015). The 2007 World Health Organization (WHO) classification of CNS tumors lists CNS-PNET NOS (not otherwise specified) and four histological CNS-PNET variants distinguished by morphological features: CNS neuroblastoma, CNS ganglioneuroblastoma, medulloepithelioma (ME), and ependymoblastoma (EB) (Louis et al., 2007). Embryonal tumors with abundant neuropil and true rosettes (ETANTR) have been

[55]Department of Hematology and Oncology, Children's University Hospital Tübingen, 72076 Tübingen, Germany

[56]Department of Neuropathology, Institute of Pathology and Neuropathology, University of Tübingen, 72076 Tübingen, Germany

[57]Department of Neuropathology, Institute of Pathology, Basel University Hospital, 4031 Basel, Switzerland

[58]Department of Pathology, Medical Center Aarau, 5001 Aarau, Switzerland

[59]Department of Pathology, University Hospital Bern, 3010 Bern, Switzerland

[60]Department of Neuropathology, Medical Center Bielefeld, 33617 Bielefeld, Germany

[61]Department of Pediatric Oncology, University Hospital Brno and Masaryk University, Faculty of Medicine, 613 00 Brno, Czech Republic

[62]Division of Molecular Histopathology, Department of Pathology, University of Cambridge, Cambridge CB2 0QQ, UK

[63]Department of Neuropathology, AMC, University of Amsterdam, 1105 AZ Amsterdam, the Netherlands

[64]Department of Neuropathology, Hôpital Sainte-Anne, 75674 Paris, France

[65]Pediatric Neurosurgery Department, Necker Enfants Malades Hospital, 75015 Paris, France

[66]Brain Tumor Program, Department of Pediatric and Adolescent Oncology, Gustave Roussy Cancer Institute, University Paris Sud, 94805 Villejuif, France

[67]Department of Pathology and Neuropathology, la Timone Hospital, AP-HM and UMR911 CR02, Aix-Marseille University, 13385 Marseille, France

[68]Department of Neuropathology, Heinrich-Heine-University, 40225 Düsseldorf, Germany

[69]German Cancer Consortium (DKTK) Partner Site Essen/Düsseldorf, 40225 Düsseldorf, Germany

[70]Section of Pediatric Neurosurgery, Department of Neurosurgery, University Hospital Tübingen, 72076 Tübingen, Germany

[71]German Cancer Consortium (DKTK) Partner Site Tübingen, 72076 Tübingen, Germany

[72]Neuro-Oncology Program, Division of Oncology, University Children's Hospital Zurich, 8032 Zürich, Switzerland

[73]Virginia Commonwealth University, Richmond, VA 23298, USA

[74]Department of Neuropathology, Institute of Pathology, University of Würzburg, 97080 Würzburg, Germany

[75]Comprehensive Cancer Center (CCC) Mainfranken, University and University Hospital, 97080 Würzburg, Germany

[76]Division of Neuropathology, Department of Pathology, NYU Langone Medical Center, New York, NY 10016, USA

[77]NYU School of Medicine, New York, NY 10016, USA

[78]Department of Oncogenomics, AMC, University of Amsterdam, 1105 AZ Amsterdam, the Netherlands

[79]Genomics and Proteomics Core Facility, High Throughput Sequencing Unit, German Cancer Research Center (DKFZ) Heidelberg, 69120 Heidelberg, Germany

[80]Departments of Neurology and Neurosurgery, Henry Ford Hospital, Detroit, MI 48202, USA

[81]Department of Oncology, St. Jude Children's Research Hospital, Memphis, TN 38105, USA

[82]Department of Neuro-Oncology, University of Texas MD Anderson Cancer Center, Houston, TX 77030, USA

[83]The University of Queensland, Brisbane, QLD 4072, Australia

[84]Children's Health Queensland Hospital and Health Service, Brisbane, QLD 4101, Australia

[85]McGill University and Genome Quebec Innovation Centre, Montreal, QC H3A 1A4, Canada

[86]Division of Pediatric Hematology/Oncology, Departments of Pediatrics and Otolaryngology, NYU Langone Medical Center and Laura and Isaac Perlmutter Cancer Center, NY 10016, New York, USA

[87]Department for Bioinformatics and Functional Genomics, Institute for Pharmacy and Molecular Biotechnology (IPMB) and BioQuant, Heidelberg University, 69120 Heidelberg, Germany

[88]Heidelberg Center for Personalized Oncology, DKFZ-HIPO, 69120 Heidelberg, Germany

[89]Co-first author

[90]Co-senior author

*Correspondence: m.kool@dkfz.de

http://dx.doi.org/10.1016/j.cell.2016.01.015

recognized as a histological variant without a specific designation. The identification of focal amplification of a micro-RNA cluster on 19q13.42 (C19MC) as a unifying feature of ME, EB, and ETANTR (Eberhart et al., 2000; Korshunov et al., 2010, 2014; Li et al., 2009; Spence et al., 2014) led to the recognition of an overarching molecular and clinicopathological entity of embryonal tumors with multi-layered rosettes (ETMR, C19MC-altered) in the next revision of the WHO classification, adding to a growing list of defining molecular aberrations in high-grade pediatric CNS tumors (Capper et al., 2010; Chan et al., 2013; Hasselblatt et al., 2013; Margol and Judkins, 2014; Pajtler et al., 2015; Parker et al., 2014; Schneppenheim et al., 2010; Schwartzentruber et al., 2012; Venneti et al., 2013; Wu et al., 2012; Yan et al., 2009).

Recent studies support the notion that CNS-PNETs represent a molecularly heterogeneous group of tumors (Danielsson et al., 2015; Picard et al., 2012; Schwalbe et al., 2013), indicating an urgent need for better methods of classification. To provide a better framework for accurate diagnosis and treatment, we performed a comprehensive molecular characterization of a large cohort of institutionally diagnosed CNS-PNETs, aiming to fully elucidate their underlying molecular and biological spectrum.

RESULTS

DNA Methylation Profiling of CNS-PNETs

We generated genome-wide DNA methylation profiles of 323 tumors with an institutional diagnosis of "CNS-PNET." Unsupervised clustering, including 211 well-characterized "reference" tumors representing other CNS tumor entities, reliably separated samples into clusters defined by histological entities and known molecular subgroups (Figures 1A, 1B, and S1A–S1D; Table S1).
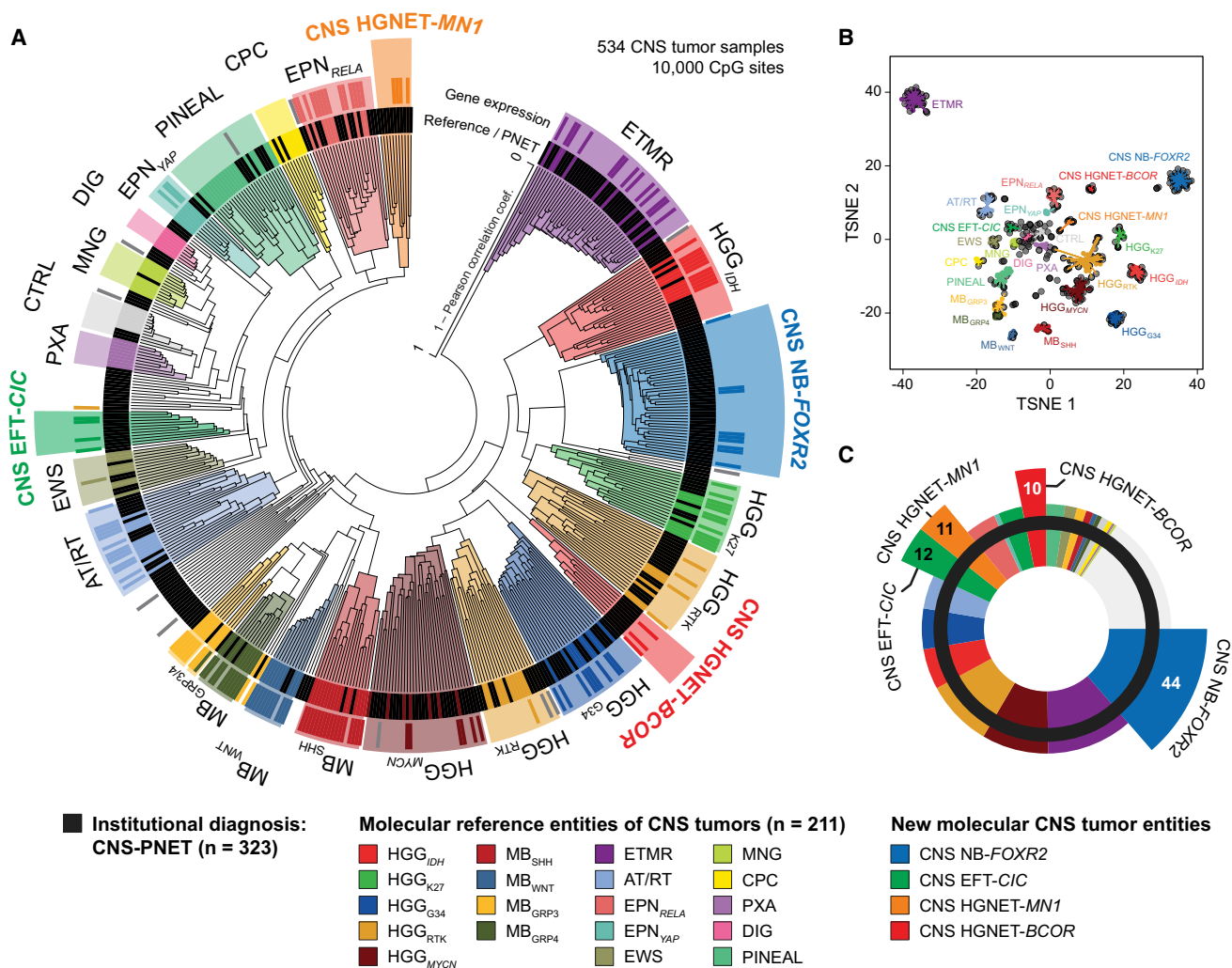
Figure 1. Molecular Classification of CNS-PNETs by DNA Methylation Profiling

(A) Unsupervised clustering of DNA methylation patterns of 323 CNS-PNET samples alongside 211 reference samples representing CNS tumors of known histology and molecular subtype using the 10,000 most variably methylated probes. Molecular diagnostic reference tumors or CNS-PNETs (inner circle) and gene expression subgroup assignment (outer circle) are depicted by colored bars as indicated. DNA methylation clusters are highlighted by colors as indicated. Gray bars indicate samples unclassifiable by gene expression analyses.

(B) 2D representation of pairwise sample correlations using the 10,000 most variably methylated probes by t-distributed stochastic neighbor embedding (tSNE) dimensionality reduction. The same samples as in (A) are used (n = 534). Reference samples are colored according to their molecular reference entity. CNS-PNET samples are colored in black. Lines connect each sample to the centroid of its respective molecular CNS tumor entity.

(C) Re-classification of 323 CNS-PNETs into known molecular reference entities and four new CNS tumor entities by molecular profiling. Entities correspond to DNA methylation clusters and are represented by colors as indicated.

See also Figure S1 and Table S1.

CNS-PNETs did not form a distinct cluster, but mostly grouped with clusters of reference CNS tumors. In total, 196/323 (61%) of CNS-PNETs clustered with ETMRs (36/323, 11%), *MYCN*-amplified high-grade gliomas (HGG$_{MYCN}$, 28/323, 9%), *IDH/H3F3A* wild-type HGG from receptor tyrosine kinase (RTK) subgroups (HGG$_{RTK}$, 28/323, 9%), *IDH* mutant HGG (HGG$_{IDH}$, 17/323, 5%), *H3F3A* G34 mutant HGG (HGG$_{G34}$, 17/323, 5%), supratentorial ependymomas (EPN, 15/323, 5%), AT/RTs (14/323, 4%), *H3F3A* K27 mutant diffuse midline gliomas (HGG$_{K27}$, 10/323, 3%), pineal tumors (PIN, 8/323, 2%), Ewing sarcomas (EWS, 5/323, 2%), choroid plexus carcinomas (CPC, 2/323, 1%), pleomorphic xanthoastrocytomas (PXA, 1/323, <1%), or meningiomas (MNG, 1/323, <1%) (Figures 1A–1C, S1A, and S1B). Some CNS-PNETs also grouped with medulloblastoma subtypes (MB$_{WNT}$, MB$_{SHH}$, MB$_{Grp3}$, MB$_{Grp4}$, 11/323, 3%), including one metastasis of a primary brainstem lesion with PNET histology. However, available radiological reports of these MB-like cases did not indicate a cerebellar lesion. Three further samples (1%) clustered with non-neoplastic hemispheric brain tissue samples, suggesting high normal cell content.

Some of the remaining CNS-PNETs (50/323, 15%) formed small, inhomogeneous clusters (<5 tumors) or represented distant outliers that failed to group with each other or any of the reference tumor entities, possibly representing exceedingly rare entities. A larger fraction of remaining CNS-PNETs (77/323, 24%) formed four separate clusters clearly distinct from reference entities. As elucidated below, these represent four new CNS tumor entities that we termed "CNS neuroblastoma with *FOXR2* activation" (CNS NB-*FOXR2*; 44/323, 14%), "CNS Ewing sarcoma family tumor with *CIC* alteration" (CNS EFT-*CIC*; 12/323, 4%), "CNS high-grade neuroepithelial tumor with *MN1* alteration" (CNS HGNET-*MN1*; 11/323, 3%), and "CNS high-grade neuroepithelial tumor with *BCOR* alteration" (CNS HGNET-*BCOR*; 10/323, 3%). Unsupervised clustering restricted to CNS-PNET samples recapitulated cluster associations established in the overall analysis (Figures S1C and S1E). For a subset of tumors (109 reference samples; 59 CNS-PNET), transcriptomic profiling allowed assignment into gene expression-based subgroups that correlated well with DNA methylation clusters (Figures 1A, S1A, and S1F).

Re-classification of CNS-PNETs into Other CNS Tumor Entities

To validate the re-classification of CNS-PNETs sharing concordant DNA methylation and transcriptomic profiles with reference tumor entities, we analyzed these samples for hallmark molecular features previously established for their assigned reference tumor entities. Only CNS-PNET samples from the ETMR cluster consistently harbored the C19MC amplicon (33/36, 92% of samples with available data; $p < 0.001$) and displayed high LIN28A protein expression (17/17, 100%; $p < 0.001$), which has been proposed as a potent diagnostic marker for ETMR (Korshunov et al., 2012, 2014; Spence et al., 2014) (Figure 2A). All analyzed CNS-PNET samples from the AT/RT cluster displayed *SMARCB1* mutations and/or deletions (14/14, 100%; $p < 0.001$) and loss of the *SMARCB1* protein product INI-1 (5/5, 100%; $p < 0.001$) (Figure 2B). Targeted sequencing confirmed mutations in *IDH1* in 15/15 CNS-PNETs (100%; $p < 0.001$) from the HGG$_{IDH}$ cluster, G34 mutations of *H3F3A* in 17/17 CNS-PNETs (100%; $p < 0.001$) from the HGG$_{G34}$ cluster, and K27 mutations of *H3F3A* in 4/7 CNS-PNETs (57%; $p < 0.001$) from the HGG$_{K27}$ cluster (Figure 2C). Within the HGG$_{MYCN}$ cluster, 20/28 CNS-PNETs (71%; $p < 0.001$) displayed amplification of the *MYCN* locus (Figure 2D). Co-amplification of *MYCN* and *ID2* was observed in 12/28 (43%; $p < 0.001$) samples, therefore broadening a previously defined molecular subgroup of diffuse intrinsic pontine gliomas (DIPG) to include supratentorial tumors with HGG or PNET histopathology (Buczkowicz et al., 2014). Where tested by fluorescence in situ hybridization (FISH; 4/4), *MYCN* and *ID2* were co-amplified in the same tumor cell nuclei (Figure 2D). CNS-PNETs within the HGG$_{RTK}$ clusters showed diverse, broad chromosomal copy-number alterations, and half (14/28, 50%) harbored focal amplifications and/or deletions of known oncogenes and/or tumor suppressor genes (Figures S2A and S2B). In the three CNS-PNETs from the EWS cluster, the presence of a *EWSR1* re-arrangement was detected by RNA sequencing or FISH analysis (data not shown). There was insufficient material to investigate CNS-PNETs from the EPN clusters for the presence of *RELA* or *YAP1* fusions. Patient information (age at diagnosis, tumor location, and survival) of CNS-PNETs from aforementioned clusters matched clinical features of their reference entities and subgroups (Figures 2E–2H and S2C–S2G).

Where available, the histology of CNS-PNETs with DNA methylation profiles and molecular markers associated with other CNS tumor entities (n = 71) was re-evaluated by an expert panel of neuropathologists. In most instances, the tumors demonstrated histological features either supporting their molecular re-classification or ambiguous histology for which the entity suggested by the molecular re-classification would be included in the differential diagnosis (Tables S2A–S2C). Among the tumors re-classified into other CNS tumor entities were small-cell tumors displaying classic features attributed to CNS-PNET (Figures S2H–S2M). These features were not restricted to the ETMR group but were also prominent in the HGG$_{G34}$ and HGG$_{MYCN}$ groups, in which specific examples demonstrated hallmark features of anaplasia, including cell wrapping and prominent nucleoli, while other tumors demonstrated diffuse infiltrative growth more typical of HGG. Rare examples of tumors re-classified into a HGG group demonstrated robust neuronal antigen expression, highlighting the insufficiency of glial and neuronal antigen expression alone to reliably discriminate these malignant small-cell CNS tumors (Figures S2N–S2P).

Identification of Four New Molecular CNS Tumor Entities

Our initial clustering analysis of CNS-PNETs identified four new molecular entities designated "CNS NB-*FOXR2*," "CNS EFT-*CIC*," "CNS HGNET-*MN1*," and "CNS HGNET-*BCOR*." To explore whether these molecular entities were also diagnosed other than CNS-PNET, we compared DNA methylation patterns of each entity with an in-house collection of >10,000 profiles from a broad variety of pediatric and adult CNS tumors (data not shown). Subsequent clustering analysis identified 59 tumors with diverse histological diagnoses that now grouped with one of the four new CNS tumor entities (Figures 3A, 3B, and S3A–S3C; Table S3). While the enlarged CNS NB-*FOXR2* (n = 46) and CNS EFT-*CIC* (n = 15) clusters represented entities with almost exclusive CNS-PNET histology (Figures 3A and 3B), the CNS HGNET-*MN1* cluster (n = 41) included 16 tumors histologically diagnosed as astroblastoma (ABM)—rare WHO-defined glial tumors—supporting the concept that they are distinct from conventional diffuse glial neoplasms (Louis et al., 2007). The CNS HGNET-*BCOR* cluster (n = 34) was expanded by a variety of CNS tumor histologies. Again, molecular subgroup assignment by transcriptomic profiling recapitulated DNA methylation-based clusters (Figures 3A and S3A) and allowed the identification of three additional tumors included in further gene expression analyses.

We correlated each of the four novel CNS tumor entities with available basic clinical parameters (Figures 3C–3F). Noticeably, the gender ratio was strongly shifted toward females in the CNS HGNET-*MN1* ($p < 0.001$), as also observed for ABM (Louis et al., 2007). Patient age at diagnosis in CNS HGNET-*MN1* was higher compared with other entities ($p < 0.001$). There were no clear differences in tumor site of occurrence, although occasional cerebellar location was restricted to tumors of the
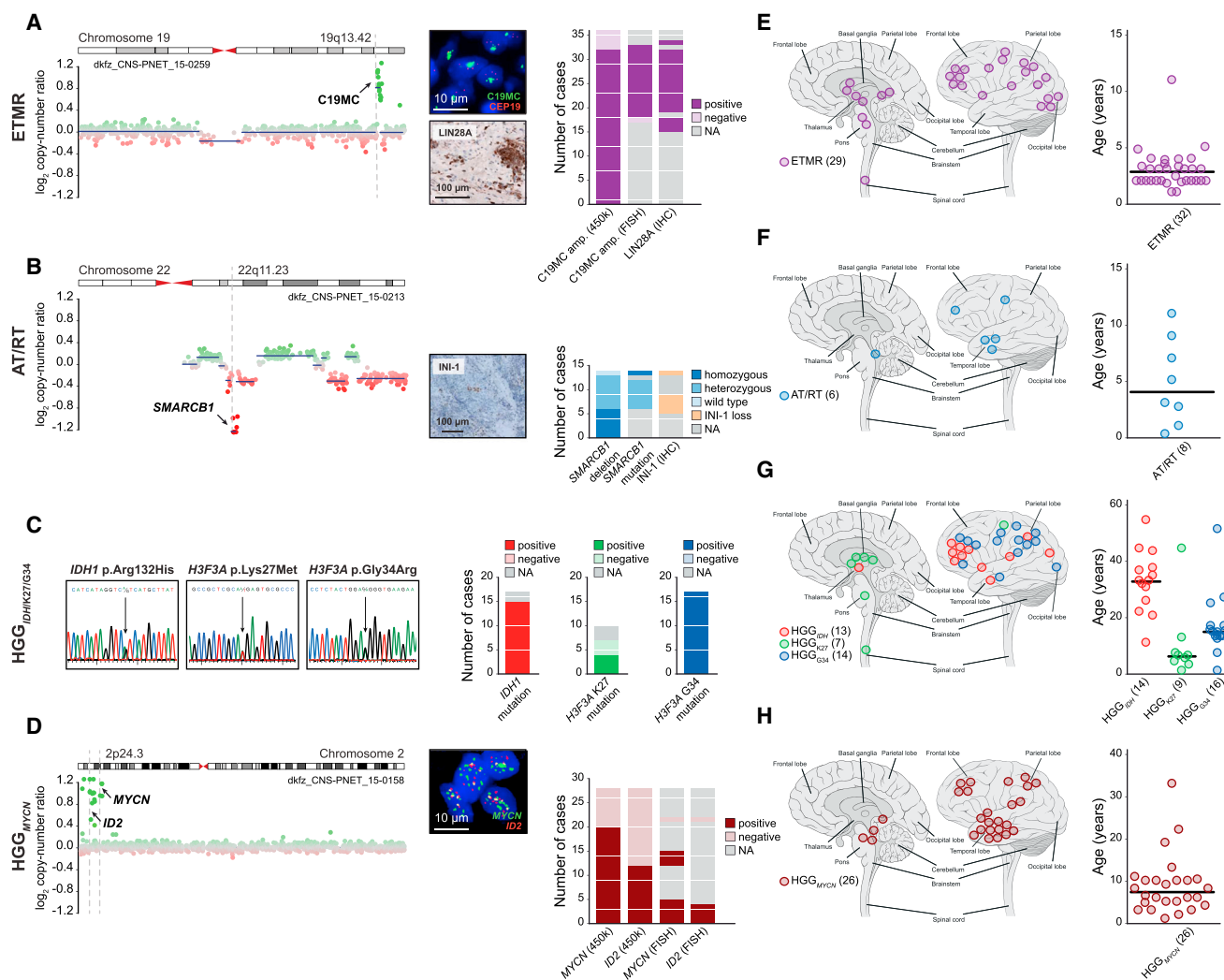
Figure 2. Molecular and Clinical Characteristics of Re-classified CNS-PNET Groups

(A–D) Molecular characteristics of CNS-PNETs from ETMR (A), AT/RT (B), HGG_{IDH}, HGG_{K27}, and HGG_{G34} (C), and HGG_{MYCN} (D) DNA methylation clusters. Detection and frequency of characteristic molecular alterations in each group is indicated. Representative copy-number profiles in (A), (B), and (D) depict genomic gains (green dots) and losses (red dots) on individual chromosomes as indicated. FISH and IHC images in (A), (B), and (D) show representative tumor samples.

(E–H) Tumor location and age at diagnosis from ETMR (E), AT/RT (F), HGG_{IDH}, HGG_{K27}, and HGG_{G34} (G), and HGG_{MYCN} (H) DNA methylation clusters. Black bars in age plots indicate the median. Numbers in brackets indicate group size with available data.

See also Figure S2 and Table S2.

CNS HGNET-*MN1* and CNS HGNET-*BCOR* entities. Infratentorial, non-cerebellar location was not associated with a specific molecular CNS tumor entity. Surgical and pathological reports of four CNS EFT-*CIC* tumors did not indicate meningeal or osseous origin. Available survival data suggested differences between the novel CNS tumor entities, with significantly better overall survival observed for patients from the CNS HGNET-*MN1* compared to the CNS HGNET-*BCOR* entity (Figure S3D).

Histopathology of New CNS Tumor Entities

Histopathological review was performed on 30 CNS NB-*FOXR2*, 14 CNS HGNET-*BCOR*, 10 CNS HGNET-*MN1*, and four CNS EFT-*CIC* tumors (Tables S2A–S2C). The CNS NB-*FOXR2* entity displayed embryonal architectural and cytological features with a small-cell phenotype (Figures 4A–4C). Areas of differentiation in the form of neuropil, neurocytic cells, or ganglion cells were observed in a high proportion of tumors (Figure 4C). Frequent perivascular anuclear zones ("vascular pseudorosettes"), nuclear palisades, and Homer Wright rosettes were encountered in individual samples (Figure S4A; Tables S2B and S2C). This group encompassed tumors that would be classified as CNS neuroblastoma or CNS ganglioneuroblastoma in the 2007 WHO classification scheme (Louis et al., 2007) (Figures 4A–4C). CNS NB-*FOXR2* tumors nearly uniformly expressed OLIG2 and the neuronal antigen synaptophysin (Figures S4A and S4B).
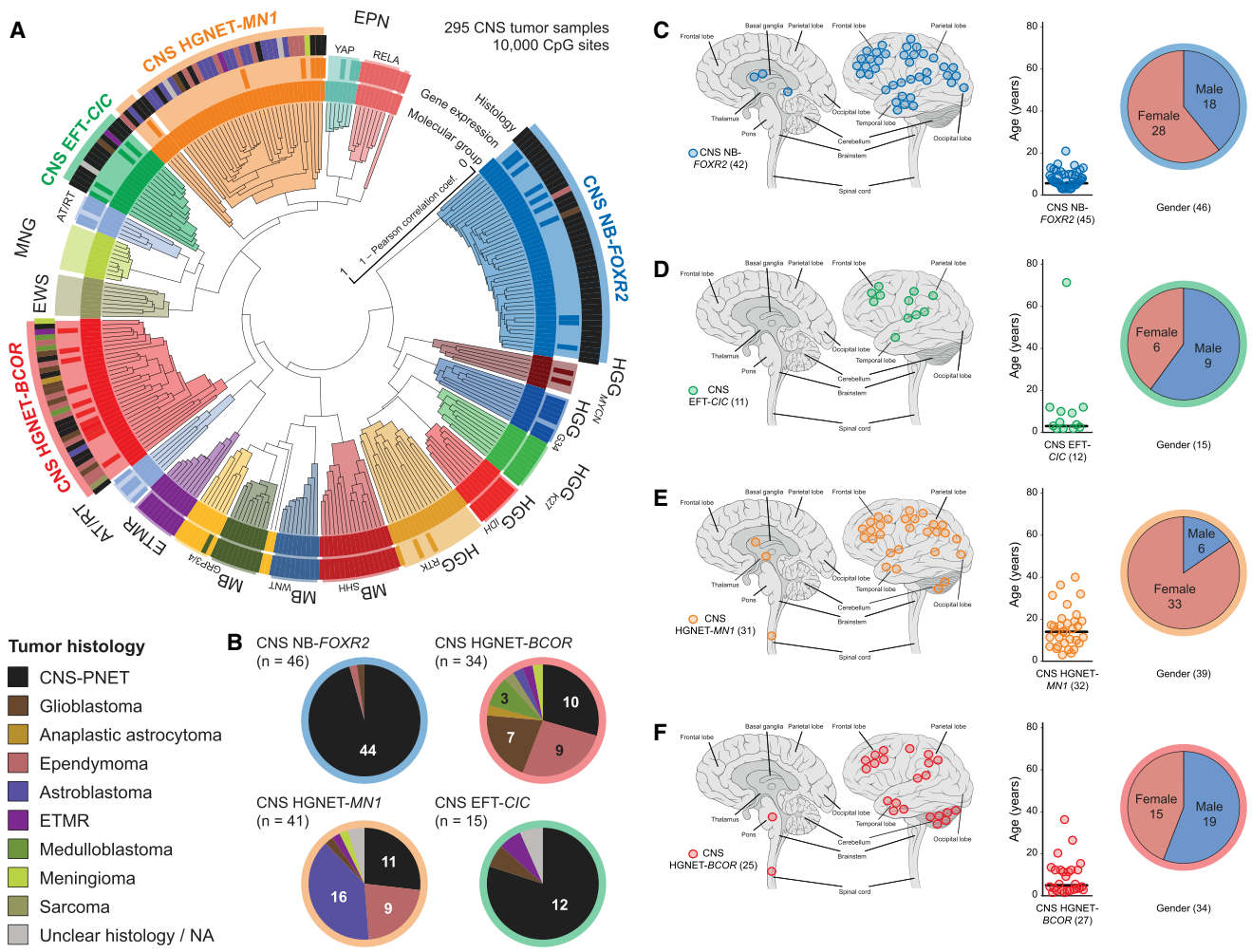
Figure 3. Identification of New CNS Tumor Entities across Histologies

(A) Unsupervised clustering of DNA methylation patterns of 77 CNS-PNET samples alongside 159 reference samples and 59 additional samples representing CNS tumors of varying histology using the 10,000 most variably methylated probes. Molecular subgroup assignment by DNA methylation (inner circle) or gene expression patterns (middle circle) correspond to subgroup labels. Original tumor histology (outer circle) is depicted for tumors from new molecular CNS tumor entities by colored bars as indicated.

(B) Composition of four new CNS tumor entities by histological diagnosis. Tumor histology is represented by colors as indicated.

(C–F) Clinical patient information for four novel CNS tumor entities CNS NB-*FOXR2* (C), CNS EFT-*CIC* (D), CNS HGNET-*MN1* (E), and CNS HGNET-*BCOR* (F). For each entity, tumor location (left), age at diagnosis (middle), and gender distribution (right) is shown. Numbers in brackets indicate group size with available data. See also Figure S3 and Table S3.

The CNS EFT-*CIC* entity was also characterized by a small-cell phenotype but with variable histology (Figures 4D–4F). The tumor architecture included both alveolar and fascicular patterns of growth. Although tumors were uniformly high grade, this group lacked defining histological features and failed to express markers of differentiation.

The CNS HGNET-*MN1* entity (Figures 4G–4I) consisted of circumscribed high-grade tumors containing a mixture of solid and pseudopapillary patterns. Dense pericellular hyalinization was frequently present in this group. Some had the typical pathology of the tumor termed astroblastoma (ABM) in the current WHO classification system, whereas others were harder to align with that diagnosis. The majority of tumors (16/23) from our current collection histologically diag-

nosed as ABM belonged to this molecular entity. Thus, we consider it unlikely that there is an additional true "astroblastoma" entity other than the *MN1*-altered entity outlined here.

The CNS HGNET-*BCOR* entity consisted of relatively compact tumors with a combination of spindle to oval cells. They often exhibited perivascular pseudorosettes, giving the tumors an ependymoma-like appearance (Figures 4J–4L). Tumors frequently demonstrated fibrillary processes, typical of glial differentiation, and only in rare instances exhibited true embryonal morphology.

Tumors from CNS HGNET-*MN1* and CNS HGNET-*BCOR* entities frequently expressed GFAP, but neuronal antigen expression was either focal or absent. In comparison, mitotic counts
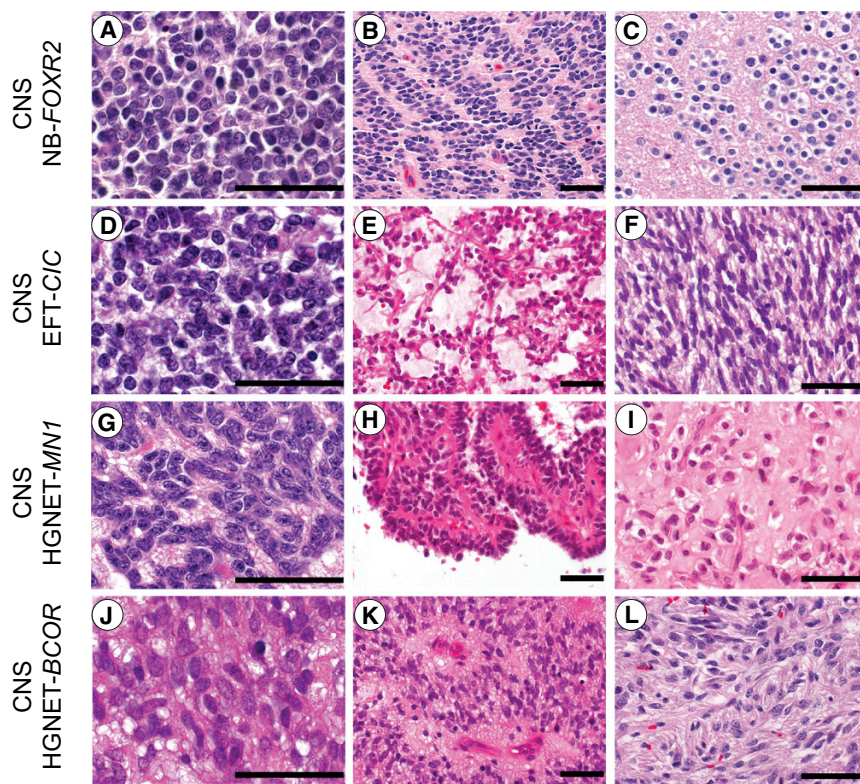
Figure 4. Histopathological Patterns of New CNS Tumor Entities

(A–C) The CNS NB-*FOXR2* entity was characterized by uniform round embryonal cells with minimal cytological pleomorphism. Nuclear palisades and neurocytic differentiation were frequently encountered.

(D–F) CNS EFT-*CIC* tumors were composed of small monotonous cells. The tumor architecture was variable and included fascicular and alveolar growth. Select examples demonstrated a spindle cell phenotype.

(G–I) CNS HGNET-*MN1* tumors were composed of monotonous neuroepithelial cells with oval forms. Pseudopapillary architecture and dense stromal hyalinization was often encountered.

(J–L) The CNS HGNET-*BCOR* entity was characterized by oval to elongated cells. Perivascular anuclear zones were often present and glial fibrillary processes were typical.

Scale bars represent 50 μm.

See also Figure S4.

were high for CNS NB-*FOXR2* and CNS EFT-*CIC* tumors, but lower for the other two entities (Figure S4C).

Genetic Alterations Define New CNS Tumor Entities

For each of the four new CNS tumor entities, we next inspected copy-number profiles derived from DNA methylation arrays. Gain of chromosome arm 1q was characteristic for the CNS NB-*FOXR2* entity (43/44, 98%; p < 0.001) (Figure S5A). Further broad aberrations included loss of 16q in CNS NB-*FOXR2* (21/42, 50%) and CNS HGNET-*MN1* (12/37, 32%), and gain of chromosome 8 in CNS NB-*FOXR2* (14/44, 32%), CNS EFT-*CIC* (3/13, 23%), and CNS HGNET-*MN1* (6/38, 16%) tumors. Most tumors from the CNS HGNET-*BCOR* entity displayed balanced copy-number profiles. We only detected high-level focal oncogene amplifications of *MYC* and *CDK4*, each in one CNS NB-*FOXR2* sample, and *EGFR* and *CDK4* in one CNS HGNET-*MN1* sample (Table S4). Homozygous deletions of *CDKN2A* were found in two CNS HGNET-*BCOR* and one CNS HGNET-*MN1* tumors.

In order to identify genetic alterations that underlie each of the four new, molecularly defined CNS tumor entities in greater detail, we performed genome-wide DNA and RNA sequencing of all cases with available fresh-frozen tissue (Table S4). As outlined below, we found that each entity was characterized by a recurrent genetic alteration.

CNS Neuroblastoma with FOXR2 Activation

Genome-wide sequencing revealed complex inter- and intra-chromosomal re-arrangements converging on *forkhead box R2* (*FOXR2*) in 6/8 samples with available data, leading to increased *FOXR2* gene expression levels in CNS NB-*FOXR2* tumors

compared with other CNS tumor entities (Figures 5A–5C). Three of the detected events resulted in fusion transcripts retaining the full coding sequence of *FOXR2*, with upstream non-coding exons forming a novel transcript variant fused to different fusion partners (Figures S5B and S5C). These included *JMJD1C* as a result of a complex inter-chromosomal translocation involving chromosome 10, and *LOC550643* and *JPX* as products of tandem duplications on chromosome X. These duplications were also detectable by characteristic copy-number changes in three samples without available sequencing data (Figure S5D). We further identified a recurrent deletion between full-length *FOXR2* and *MAGEH1* in two samples. Copy-number data indicated additional alterations targeting the *FOXR2* locus in seven samples (Figure S5D), with a deletion reaching ∼500 kb upstream of *FOXR2* as the most frequent event (4/46, 9%), potentially fusing *FOXR2* to the *MAGED2* gene.

Moreover, we identified a mitochondrial DNA insertion within *USP51* that led to the formation of a novel *FOXR2* promoter (Figure S5E). Mitochondrial-nuclear genome fusions have been recently reported to occur frequently in cancer (Ju et al., 2015), but this is the first example in which such an event induces oncogene expression. Since *FOXR2* is not expressed in other CNS tumor types (Figure 5C) or normal brain tissues, these events are suggestive of *FOXR2* activation facilitated by promoters of active genes (Figure S5F), thus instigating oncogenic activity (Rahrmann et al., 2013). One exceptional tumor that did not show elevated gene expression of *FOXR2* was the only one to harbor a focal amplification of *MYC*, resulting in upregulated *MYC* gene expression compared with *FOXR2*-activated tumors (Figure S5F). The *FOXR2* homolog *FOXR1* is recurrently activated in peripheral neuroblastoma counterparts by intrachromosomal deletion/fusion events, resulting in overexpression of fusion transcripts (Santo et al., 2012).
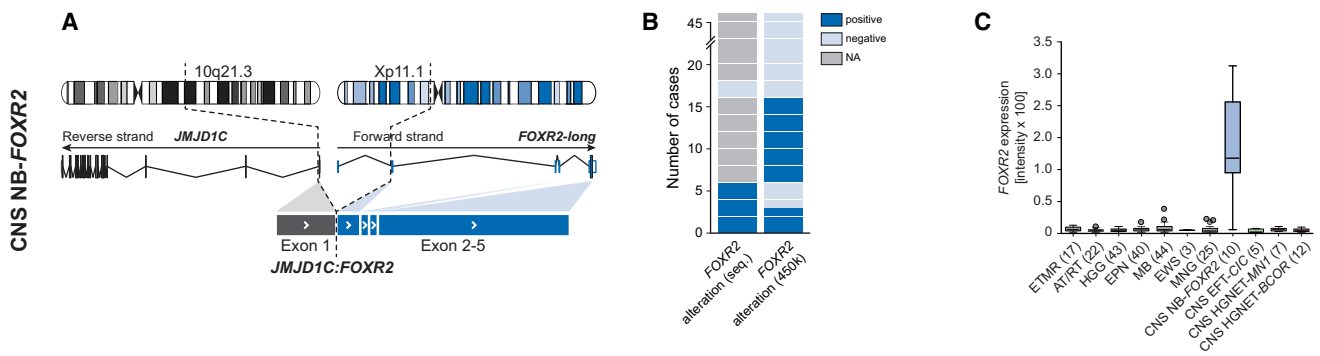
Figure 5. Recurrent Molecular Alterations in the CNS NB-*FOXR2* Entity

(A) Schematic representation depicting chromosomal location, wild-type RNA transcripts, and exon structures resulting from an exemplary genetic alteration affecting the *FOXR2* gene.

(B) Frequency of *FOXR2* re-arrangements identified by RNA/DNA sequencing or copy-number data.

(C) Gene expression levels of *FOXR2* in various CNS tumor entities.

See also Figure S5 and Table S4.

CNS Ewing Sarcoma Family Tumor with CIC Alteration

In three tumors analyzed by RNA sequencing we detected an interchromosomal gene fusion between *capicua transcriptional repressor* (*CIC*, located on chromosome 19q13.2) and *NUT midline carcinoma, family member 1* (*NUTM1*, located on chromosome 15q14) in two samples (Figures 6A, 6B, and S6A), while the third harbored a frameshift deletion in *CIC* (exon6: c.902delC:p.S301fs). Both fusion events fused exon 16 of *CIC* in-frame to exon 4 of *NUTM1*, retaining the DNA-binding high mobility group (HMG) box domain of CIC. Using a *CIC* break-apart FISH probe, we identified *CIC* re-arrangements in 8/9 samples, including one of the tumors analyzed by RNA sequencing (Figures 6B and S6B), while the FISH-negative tumor carried the *CIC* frameshift deletion. Gene expression data indicated transcriptional upregulation of fusion partner *NUTM1* in this group compared with all other samples (Figure 6C). Consequently, those tumors showed strong reactivity when investigated for NUTM1 protein expression by immunohistochemistry, while no tumors from any other entity stained positive (Figures 6B, S4A, and S4B). On the basis of *CIC* fusions present in subgroups of pediatric primitive round cell sarcomas (Haidar et al., 2015) and their distinct transcriptional signature (Specht et al., 2014), we analyzed CNS EFT-*CIC* tumors for similar gene expression patterns. As observed in peripheral EFT, among the genes specifically upregulated in this group were members of the ETS transcription factor family, including *ETV1*, *ETV4*, *ETV5*, *FLI1*, and *ETS1* (Figure S6C). Oncogenic re-arrangements of *NUTM1* are a defining genetic feature of NUT midline carcinomas (NMC), in most cases involving *bromodomain-containing protein 4* (*BRD4*) (French, 2014). We hypothesize a molecular mode of action of *CIC-NUTM1* fusions in which specific *CIC* target genes are transcriptionally activated by the NUTM1 moiety via the recruitment of histone acetyl transferases, similar to a model of how BRD4-NUTM1 might block differentiation in NMC (French, 2014). As this may lead to global hypoacetylation, these findings provide a rationale for testing the efficacy of epigenetically active drugs in this tumor entity.

CNS High-Grade Neuroepithelial Tumor with MN1 Alteration

We identified interchromosomal gene fusions between *meningioma (disrupted in balanced translocation) 1* (*MN1*, 22q12.3) and *BEN domain containing 2* (*BEND2*, Xp22.13) in three samples, and *MN1* and *CXXC-type zinc-finger protein 5* (*CXXC5*, 5q31.2) in one sample (Figures 6D, 6E, and S6D) from RNA sequencing data of four tumors. Using an *MN1* break-apart FISH probe, *MN1* re-arrangement was confirmed in three of the tumors with RNA sequencing data and nine additional tumors from the CNS HGNET-*MN1* entity (Figures 6E and S6E). High-level gene expression of the fusion partner *BEND2* was observed specifically in CNS HGNET-*MN1* tumors, while being absent in other CNS tumor types (Figure 6F). BEND2 immunohistochemistry failed to give reliable results due to non-specific staining with available antibodies. In the tumor with *MN1-CXXC5* fusion, *CXXC5* but not *BEND2*, was expressed at high levels (data not shown). A smaller set of five samples, including the tumor harboring the *MN1-CXXC5* fusion, formed a distinctly separate cluster, while all three tumors harboring an *MN1-BEND2* fusion were found in a larger homogenous cluster, potentially indicating differences in underlying biology depending on the *MN1* fusion partner (Figures 3A and S3A). The gender bias was even more striking in the two separated clusters (male:female ratio: 2:32, p < 0.001; and 4:1, respectively). Fused to *BEND2*, the encoded chimeric protein combines the transactivating domains of MN1 and the two BEN domains in the C terminus of BEND2, which have been suggested to mediate protein-DNA and protein-protein interactions during chromatin organization and transcription (Abhiman et al., 2008). In myeloid leukemia, frequently occurring MN1-TEL fusion proteins act as transcription factors with transforming activity both via targeting TEL binding sites (Buijs et al., 2000) and a dominant-negative effect on wild-type MN1 (van Wely et al., 2007).

CNS High-Grade Neuroepithelial Tumor with BCOR Alteration

DNA and RNA sequencing revealed in-frame internal tandem duplications of the *BCL6 corepressor* (*BCOR*) in 10/10 (100%)
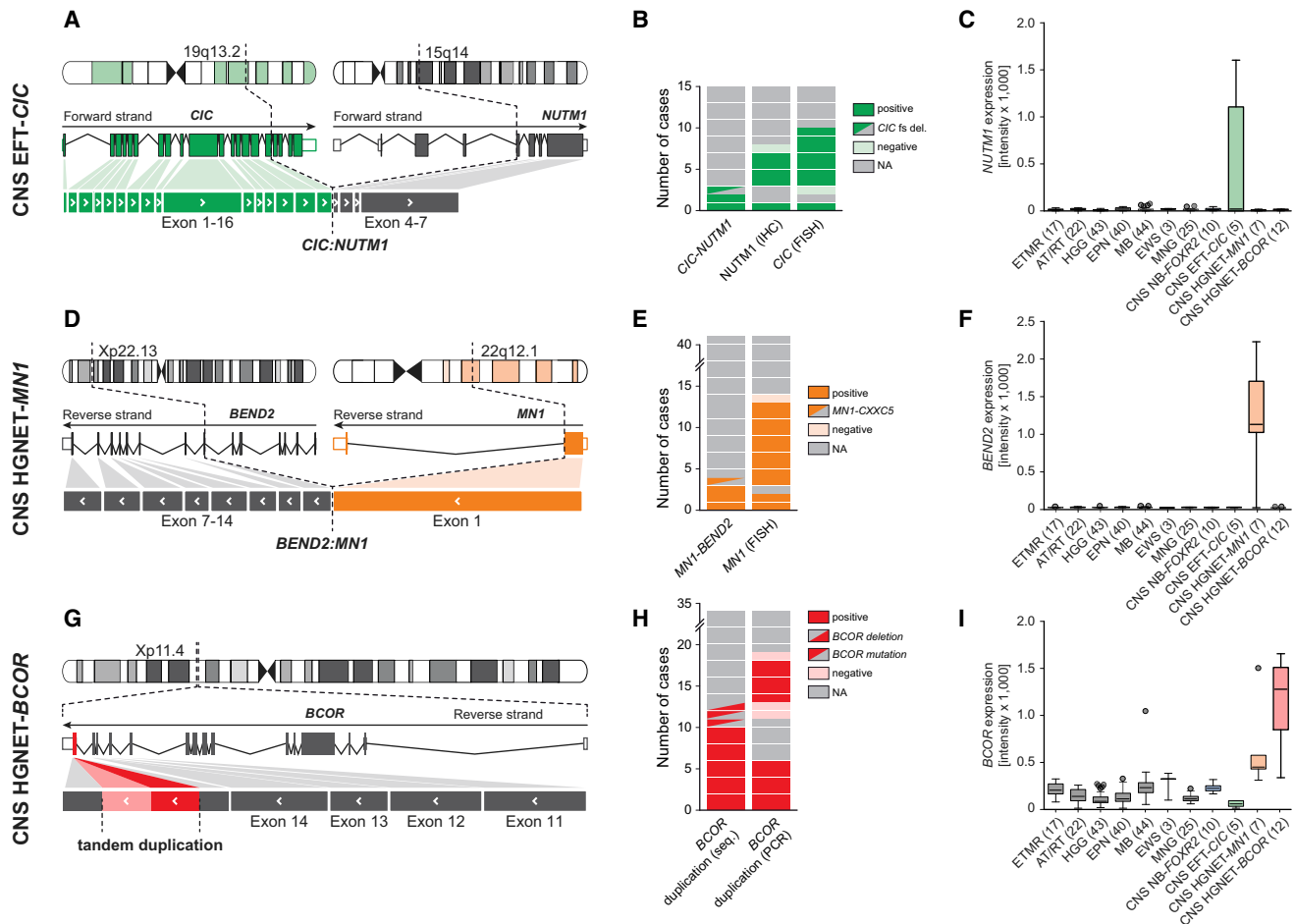
Figure 6. Recurrent Molecular Alterations in CNS EFT-*CIC*, CNS HGNET-*MN1*, and CNS HGNET-*BCOR* Entities

(A–I) Schematic representation, frequency, and transcriptomic effects of recurrent molecular alterations found in tumors from the CNS EFT-*CIC* (A–C), CNS HGNET-*MN1* (D–F), and CNS HGNET-*BCOR* (G–I) entities. Schematics in (A), (D), and (G) depict chromosomal location, wild-type RNA transcripts, and exon structures resulting from recurrent alterations. The frequencies of the respective events detected by different methods are depicted in (B), (E), and (H). Gene expression levels of *NUTM1*, *BEND2*, and *BCOR* across various CNS tumor entities are displayed in (C), (F), and (I).

See also Figure S6 and Table S4.

samples (Figures 6G, 6H, and S6F). The duplicated region in exon 15 of *BCOR* was identical with that of *BCOR* tandem duplications recently described in clear cell sarcomas of the kidney (Ueno-Yokohata et al., 2015) (Figure S6G). One additional tumor harbored an intragenic in-frame deletion in *BCOR* fusing the previous exon directly to the sequence duplicated in the other samples (Figure S6F), while two more tumors from that entity carried *BCOR* frameshift mutations. Duplications in *BCOR* were detected by targeted PCR in five additional tumors (Figures 6H and S6G). Activation of the WNT signaling pathway as indicated by nuclear beta-catenin immunoreactivity was observed in 11/14 samples (79%) (Figures S4A and S4B). Gene expression of *BCOR* was found at higher levels in CNS HGNET-*BCOR* tumors than in most other CNS tumor types (Figure 6I). High expression of altered *BCOR* transcripts in CNS HGNET-*BCOR* tumors suggests a mechanism different from *BCOR* loss-of-function mutations reported in other malignancies, such as medulloblastoma (Jones et al., 2012; Pugh et al., 2012).

Differential Pathway Activation in New CNS Tumor Entities

Array-based gene expression analyses of tumors from the four new entities (n = 34) identified many genes (range: 435–2,880) as significantly (adj. p < 0.001) differentially expressed between one versus the other three entities (Table S5). Subsets of these genes, which frequently included transcription factors and potential drug targets, showed upregulated expression within the new entities (Figures 7A and S7A), suggesting activation of specific pathways or transcriptional networks (Figure S7B), and were also often not expressed in other CNS tumor entities (Figure 7B). Gene-ranked pathway enrichment analysis (Reimand et al., 2011) of entity-specific genes relative to non-neoplastic brain tissues indicated several general and specific neuronal developmental processes being activated similarly in each of the four entities, but also identified deregulated processes and pathways more unique to one or more of the entities (Figure S7C; Tables S6A–S6D).
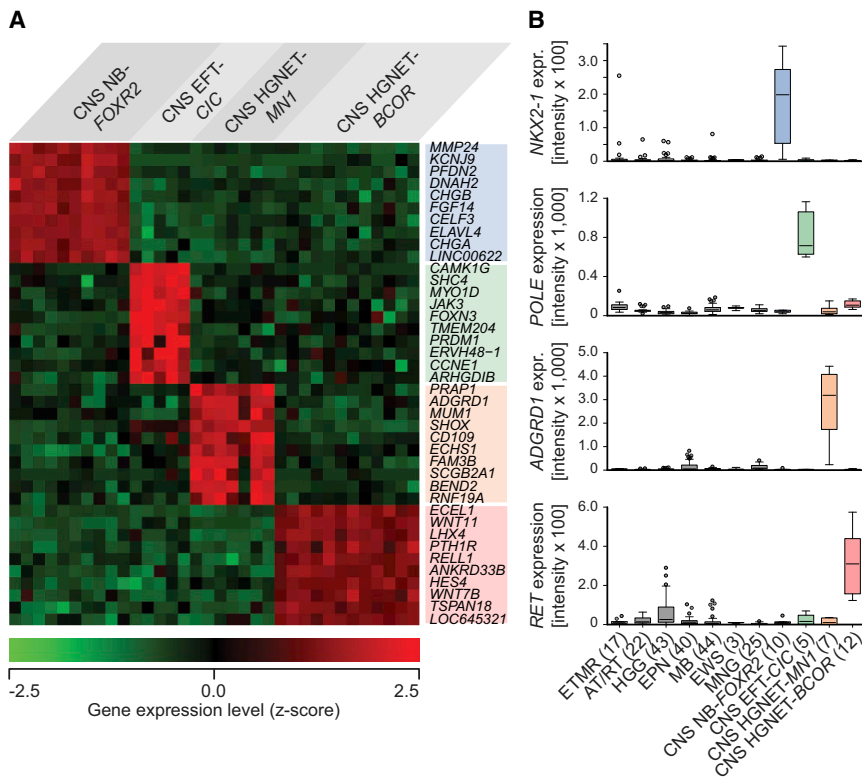
Figure 7. Transcriptional Profiling of New CNS Tumor Entities

(A) Heatmap representing the expression levels of the ten most significantly differentially upregulated genes comparing one new CNS tumor entity versus the three others. Each column represents one sample, and each lane represents one gene. Gene expression levels are represented by a color scale as indicated.

(B) Individually selected marker genes specifically upregulated in one of the new CNS tumor entities compared with other CNS tumor entities as indicated.

See also Figure S7 and Tables S5 and S6.

tiatives accumulate larger tumor series, our approach has potential to expand the molecular classification of malignant brain tumors, pushing the limits of what is recognized as a bona fide entity.

In conclusion, our findings reinforce the importance of incorporating molecular information into the next revision of the WHO classification of CNS tumors (Louis et al., 2014) and warrant a replacement of the term "CNS-PNET" with biologically specific designations. Our study provides an innovative framework for improving diagnostic accuracy and prognostication in malignant CNS tumors. The approach is amenable to retrospective analyses of patients treated with current regimens and will facilitate the design of more meaningful clinical trials for patients with malignant brain tumors.

DISCUSSION

Our study demonstrates that the embryonal histology of CNS-PNETs does not correspond to a homogeneous molecular class and suggests that a majority of tumors designated CNS-PNET represent morphological variants of other histologically and molecularly defined diagnostic entities. While a subset of tumors diagnosed as CNS-PNET were questionable or inaccurate diagnoses upon expert review, a high proportion of tumors demonstrated ambiguous small-cell morphology that was difficult to classify on histology alone, highlighting the diagnostic necessity of utilizing established molecular markers.

Our study also led to the identification of four new molecularly defined CNS tumor entities. The entity designated "CNS neuroblastoma with *FOXR2* activation" consisted of a relatively pure population of CNS-PNET and was enriched for CNS-PNET variants CNS neuroblastoma and ganglioneuroblastoma. This entity therefore clarifies the molecular underpinnings of histopathological CNS-PNET variants into two primary entities, namely, ETMR (which accounts for the previously described ETANTR, ME, and EB) and CNS NB-*FOXR2*. We have further defined three additional molecular entities among pediatric CNS tumors, of which one entity, CNS HGNET-*MN1*, incorporates astroblastomas, while CNS EFT-*CIC* and CNS HGNET-*BCOR* represent novel entities displaying pathological overlap with CNS-PNET and other histological entities.

A minority of CNS-PNETs failed to classify into a specific subgroup, therefore representing a group we currently consider as "CNS embryonal tumors, NOS." However, as international ini-

EXPERIMENTAL PROCEDURES

Tumor samples and clinical data were collected at the DKFZ (Heidelberg, Germany) and at the St. Jude Children's Research Hospital (Memphis) in accordance with research ethics board approval from both institutes. Additional tumor samples and clinical data were provided by collaborating centers world-wide. Clinical patient details can be found in Tables S1A and S3. An overview of all CNS-PNET and other CNS tumor samples included in various analyses is given within the Supplemental Experimental Procedures. Inclusion criteria for CNS-PNET samples comprised an institutional diagnosis of "CNS-PNET" (excluding medulloblastoma) and sufficient high-quality DNA for methylation profiling. Wherever possible, H&E-stained formalin-fixed paraffin-embedded (FFPE) sections from CNS-PNET and additional CNS tumor samples were reviewed by experienced neuropathologists (A.K., D.W.E., B.A.O., D.C.; n = 151; see Table S2).

DNA methylation profiling of CNS-PNET and reference samples was performed from both fresh-frozen and FFPE tissue using the Infinium Human-Methylation450 BeadChip Array (450k array) in accordance with the manufacturer's instructions (Illumina). For unsupervised hierarchical clustering of CNS-PNET and reference samples, we selected the 10,000 most variably methylated probes across the dataset. Copy-number variation (CNV) analysis from 450k methylation array data was performed using the conumee Bioconductor package (v.1.0.0). Scoring of focal amplifications and deletions and chromosomal gains and losses was performed by manual inspection of each profile.

Samples for which RNA of sufficient quantity and quality was available were analyzed on the Affymetrix GeneChip Human Genome U133 Plus (v.2.0) Array

(Affymetrix). Sample library preparation, hybridization, and quality control were performed in accordance with the manufacturer's protocols.

Next-generation DNA and RNA sequencing was performed using Illumina technologies as previously described (Jones et al., 2012). In addition to automated detection of alterations, candidate genes and their 3′ and 5′ intergenic neighborhood were manually investigated using the Integrative Genomics Viewer (IGV) (Robinson et al., 2011) for any breakpoints.

A detailed description of each analysis presented in this study can be found within the Supplemental Experimental Procedures.

ACCESSION NUMBERS

The sequencing data reported in this paper have been uploaded to European Genome-phenome Archive (EGA; http://www.ebi.ac.uk/ega/) under accession number EGAS00001001632. The gene expression data reported in this paper have been uploaded to NCBI's Gene Expression Omnibus (GEO; http://www.ncbi.nlm.nih.gov/geo) under accession number GEO: GSE73038. CpG methylation values reported in this paper have been uploaded to NCBI's GEO under accession number GEO: GSE73801.

SUPPLEMENTAL INFORMATION

Supplemental Information includes Supplemental Experimental Procedures, seven figures, and six tables and can be found with this article online at http://dx.doi.org/10.1016/j.cell.2016.01.015.

AUTHOR CONTRIBUTIONS

D. Sturm, B.A.O., U.H.T. and V. Hovestadt contributed equally to this manuscript. S.M.P., D.W.E., A.K., and M.K. conceived of the project. D. Sturm, B.A.O., U.H.T., V. Hovestadt, D.W.E., A.K., and M.K. wrote the manuscript with input from all co-authors. D. Sturm, B.A.O., S.W., D.W.E., and M.K. coordinated data generation. V. Hovestadt and M. Sill analyzed DNA methylation microarray data. U.H.T., I.B., G.B., B.C.W., A.M., D.M.C., R.E., and M. Schlesner analyzed genome-wide sequencing data. J.K., R. Versteeg, R. Volckmann, and P. van Sluis conducted gene expression microarray analyses. V. Hovestadt, J. Reimand, J.K., and M.K. analyzed gene expression microarray data. B.A.O., D.C., F.G., P.V., D.F.-B., G.R., V.P.C., A.v.D., D.W.E., and A.K. reviewed tumor histology. D. Sturm, B.A.O., P.A.N., I.L., M. Ryzhova, C. Koelsche, E.P., S.J.A., K.W.P., S.B., P.D.J., F.S., R.S., and A.K. performed validation experiments. D. Sturm, B.A.O., U.H.T., V. Hovestadt, D.T.W.J., P.A.N., M. Schlesner, P.L., S.M.P., D.W.E., A.K., and M.K. collected and interpreted data. M. Ryzhova, M. Remke, J.J.P., A.P., C.C., R.D., M.F., F.G., M.Ł., W.G., W.S., T.P., C. Hagel, J. Gojo, D.L., W.B., I.S., C. Haberler, A.J., S. Holm, S. Hofer, M.P., C. Keohane, I.F., C.M., D. Scheie, B.C.M., M.J.S., M. Santi, A.M.B., S.D., C.M.K., A.O.v.B., K.v.H., S.R., C.H.-M., M.C.F., T. Milde, M.H., P.W., J. Rößler, U.S., M.E., J.S., S.F., R.G., I.V., V. Hans, K.Z., V.P.C., E.A., P.V., S.P., C.D., J. Grill, M.W., M.U.S., T.S., M.G., T.v.M., C.-M.M., W.R., J.F., G.R., M. Snuderl, L.A.F., T. Mikkelsen, A.G., K.A., M.D.T., A.M., C.J., N.J., M.A.K., A.v.D., D.W.E., and A.K. provided tumor samples and metadata. All co-authors contributed to the final manuscript.

ACKNOWLEDGMENTS

REFERENCES

Abhiman, S., Iyer, L.M., and Aravind, L. (2008). BEN: a novel domain in chromatin factors and DNA viral proteins. Bioinformatics 24, 458–461.

Buczkowicz, P., Hoeman, C., Rakopoulos, P., Pajovic, S., Letourneau, L., Dzamba, M., Morrison, A., Lewis, P., Bouffet, E., Bartels, U., et al. (2014). Genomic analysis of diffuse intrinsic pontine gliomas identifies three molecular subgroups and recurrent activating ACVR1 mutations. Nat. Genet. 46, 451–456.

Buijs, A., van Rompaey, L., Molijn, A.C., Davis, J.N., Vertegaal, A.C., Potter, M.D., Adams, C., van Baal, S., Zwarthoff, E.C., Roussel, M.F., and Grosveld, G.C. (2000). The MN1-TEL fusion protein, encoded by the translocation (12;22)(p13;q11) in myeloid leukemia, is a transcription factor with transforming activity. Mol. Cell. Biol. 20, 9281–9293.

Capper, D., Weissert, S., Balss, J., Habel, A., Meyer, J., Jäger, D., Ackermann, U., Tessmer, C., Korshunov, A., Zentgraf, H., et al. (2010). Characterization of R132H mutation-specific IDH1 antibody binding in brain tumors. Brain Pathol. 20, 245–254.

Chan, K.M., Fang, D., Gan, H., Hashizume, R., Yu, C., Schroeder, M., Gupta, N., Mueller, S., James, C.D., Jenkins, R., et al. (2013). The histone H3.3K27M mutation in pediatric glioma reprograms H3K27 methylation and gene expression. Genes Dev. 27, 985–990.

Danielsson, A., Nemes, S., Tisell, M., Lannering, B., Nordborg, C., Sabel, M., and Carén, H. (2015). MethPed: a DNA methylation classifier tool for the identification of pediatric brain tumor subtypes. Clin. Epigenetics 7, 62.

Eberhart, C.G., Brat, D.J., Cohen, K.J., and Burger, P.C. (2000). Pediatric neuroblastic brain tumors containing abundant neuropil and true rosettes. Pediatr. Dev. Pathol. 3, 346–352.

French, C. (2014). NUT midline carcinoma. Nat. Rev. Cancer 14, 149–150.

Haidar, A., Arekapudi, S., DeMattia, F., Abu-Isa, E., and Kraut, M. (2015). High-grade undifferentiated small round cell sarcoma with t(4;19)(q35;q13.1) CIC-DUX4 fusion: emerging entities of soft tissue tumors with unique histopathologic features–a case report and literature review. Am. J. Case Rep. 16, 87–94.

Hasselblatt, M., Isken, S., Linge, A., Eikmeier, K., Jeibmann, A., Oyen, F., Nagel, I., Richter, J., Bartelheim, K., Kordes, U., et al. (2013). High-resolution genomic analysis suggests the absence of recurrent genomic alterations other than SMARCB1 aberrations in atypical teratoid/rhabdoid tumors. Genes Chromosomes Cancer 52, 185–190.

Jakacki, R.I., Burger, P.C., Kocak, M., Boyett, J.M., Goldwein, J., Mehta, M., Packer, R.J., Tarbell, N.J., and Pollack, I.F. (2015). Outcome and prognostic factors for children with supratentorial primitive neuroectodermal tumors treated with carboplatin during radiotherapy: a report from the Children's Oncology Group. Pediatr. Blood Cancer 62, 776–783.

Jones, D.T.W., Jäger, N., Kool, M., Zichner, T., Hutter, B., Sultan, M., Cho, Y.J., Pugh, T.J., Hovestadt, V., Stütz, A.M., et al. (2012). Dissecting the genomic complexity underlying medulloblastoma. Nature 488, 100–105.

Ju, Y.S., Tubio, J.M., Mifsud, W., Fu, B., Davies, H.R., Ramakrishna, M., Li, Y., Yates, L., Gundem, G., Tarpey, P.S., et al.; ICGC Prostate Cancer Working Group; ICGC Bone Cancer Working Group; ICGC Breast Cancer Working Group (2015). Frequent somatic transfer of mitochondrial DNA into the nuclear genome of human cancer cells. Genome Res. 25, 814–824.

Korshunov, A., Remke, M., Gessi, M., Ryzhova, M., Hielscher, T., Witt, H., Tobias, V., Buccoliero, A.M., Sardi, I., Gardiman, M.P., et al. (2010). Focal genomic amplification at 19q13.42 comprises a powerful diagnostic marker for embryonal tumors with ependymoblastic rosettes. Acta Neuropathol. 120, 253–260.

Korshunov, A., Ryzhova, M., Jones, D.T., Northcott, P.A., van Sluis, P., Volckmann, R., Koster, J., Versteeg, R., Cowdrey, C., Perry, A., et al. (2012). LIN28A immunoreactivity is a potent diagnostic marker of embryonal tumor with multilayered rosettes (ETMR). Acta Neuropathol. 124, 875–881.

Korshunov, A., Sturm, D., Ryzhova, M., Hovestadt, V., Gessi, M., Jones, D.T., Remke, M., Northcott, P., Perry, A., Picard, D., et al. (2014). Embryonal tumor with abundant neuropil and true rosettes (ETANTR), ependymoblastoma, and medulloepithelioma share molecular similarity and comprise a single clinicopathological entity. Acta Neuropathol. 128, 279–289.

Li, M., Lee, K.F., Lu, Y., Clarke, I., Shih, D., Eberhart, C., Collins, V.P., Van Meter, T., Picard, D., Zhou, L., et al. (2009). Frequent amplification of a chr19q13.41 microRNA polycistron in aggressive primitive neuroectodermal brain tumors. Cancer Cell 16, 533–546.

Louis, D.N., Ohgaki, H., Wiestler, O.D., and Cavenee, W.K. (2007). WHO Classification of Tumors of the Central Nervous System (IARC Press).

Louis, D.N., Perry, A., Burger, P., Ellison, D.W., Reifenberger, G., von Deimling, A., Aldape, K., Brat, D., Collins, V.P., Eberhart, C., et al.; International Society of Neuropathology–Haarlem (2014). International Society of Neuropathology–Haarlem consensus guidelines for nervous system tumor classification and grading. Brain Pathol. 24, 429–435.

Margol, A.S., and Judkins, A.R. (2014). Pathology and diagnosis of SMARCB1-deficient tumors. Cancer Genet. 207, 358–364.

Pajtler, K.W., Witt, H., Sill, M., Jones, D.T., Hovestadt, V., Kratochwil, F., Wani, K., Tatevossian, R., Punchihewa, C., Johann, P., et al. (2015). Molecular classification of ependymal tumors across all CNS compartments, histopathological grades, and age groups. Cancer Cell 27, 728–743.

Parker, M., Mohankumar, K.M., Punchihewa, C., Weinlich, R., Dalton, J.D., Li, Y., Lee, R., Tatevossian, R.G., Phoenix, T.N., Thiruvenkatam, R., et al. (2014). C11orf95-RELA fusions drive oncogenic NF-κB signalling in ependymoma. Nature 506, 451–455.

Picard, D., Miller, S., Hawkins, C.E., Bouffet, E., Rogers, H.A., Chan, T.S., Kim, S.K., Ra, Y.S., Fangusaro, J., Korshunov, A., et al. (2012). Markers of survival and metastatic potential in childhood CNS primitive neuro-ectodermal brain tumours: an integrative genomic analysis. Lancet Oncol. 13, 838–848.

Pugh, T.J., Weeraratne, S.D., Archer, T.C., Pomeranz Krummel, D.A., Auclair, D., Bochicchio, J., Carneiro, M.O., Carter, S.L., Cibulskis, K., Erlich, R.L., et al. (2012). Medulloblastoma exome sequencing uncovers subtype-specific somatic mutations. Nature 488, 106–110.

Rahrmann, E.P., Watson, A.L., Keng, V.W., Choi, K., Moriarity, B.S., Beckmann, D.A., Wolf, N.K., Sarver, A., Collins, M.H., Moertel, C.L., et al. (2013). Forward genetic screen for malignant peripheral nerve sheath tumor formation identifies new genes and pathways driving tumorigenesis. Nat. Genet. 45, 756–766.

Reimand, J., Arak, T., and Vilo, J. (2011). g:Profiler–a web server for functional interpretation of gene lists (2011 update). Nucleic Acids Res. 39, W307–W315.

Robinson, J.T., Thorvaldsdóttir, H., Winckler, W., Guttman, M., Lander, E.S., Getz, G., and Mesirov, J.P. (2011). Integrative genomics viewer. Nat. Biotechnol. 29, 24–26.

Rorke, L.B. (1983). The cerebellar medulloblastoma and its relationship to primitive neuroectodermal tumors. J. Neuropathol. Exp. Neurol. 42, 1–15.

Rorke, L.B., Trojanowski, J.Q., Lee, V.M., Zimmerman, R.A., Sutton, L.N., Biegel, J.A., Goldwein, J.W., and Packer, R.J. (1997). Primitive neuroectodermal tumors of the central nervous system. Brain Pathol. 7, 765–784.

Santo, E.E., Ebus, M.E., Koster, J., Schulte, J.H., Lakeman, A., van Sluis, P., Vermeulen, J., Gisselsson, D., Øra, I., Lindner, S., et al. (2012). Oncogenic activation of FOXR1 by 11q23 intrachromosomal deletion-fusions in neuroblastoma. Oncogene 31, 1571–1581.

Schneppenheim, R., Frühwald, M.C., Gesk, S., Hasselblatt, M., Jeibmann, A., Kordes, U., Kreuz, M., Leuschner, I., Martin Subero, J.I., Obser, T., et al. (2010). Germline nonsense mutation and somatic inactivation of SMARCA4/BRG1 in a family with rhabdoid tumor predisposition syndrome. Am. J. Hum. Genet. 86, 279–284.

Schwalbe, E.C., Hayden, J.T., Rogers, H.A., Miller, S., Lindsey, J.C., Hill, R.M., Nicholson, S.L., Kilday, J.P., Adamowicz-Brice, M., Storer, L., et al. (2013). Histologically defined central nervous system primitive neuro-ectodermal tumours (CNS-PNETs) display heterogeneous DNA methylation profiles and show relationships to other paediatric brain tumour types. Acta Neuropathol. 126, 943–946.

Schwartzentruber, J., Korshunov, A., Liu, X.Y., Jones, D.T.W., Pfaff, E., Jacob, K., Sturm, D., Fontebasso, A.M., Quang, D.A., Tönjes, M., et al. (2012). Driver mutations in histone H3.3 and chromatin remodelling genes in paediatric glioblastoma. Nature 482, 226–231.

Specht, K., Sung, Y.S., Zhang, L., Richter, G.H., Fletcher, C.D., and Antonescu, C.R. (2014). Distinct transcriptional signature and immunoprofile of CIC-DUX4 fusion-positive round cell tumors compared to EWSR1-rearranged Ewing sarcomas: further evidence toward distinct pathologic entities. Genes Chromosomes Cancer 53, 622–633.

Spence, T., Sin-Chan, P., Picard, D., Barszczyk, M., Hoss, K., Lu, M., Kim, S.K., Ra, Y.S., Nakamura, H., Fangusaro, J., et al. (2014). CNS-PNETs with C19MC amplification and/or LIN28 expression comprise a distinct histogenetic diagnostic and therapeutic entity. Acta Neuropathol. 128, 291–303.

Ueno-Yokohata, H., Okita, H., Nakasato, K., Akimoto, S., Hata, J., Koshinaga, T., Fukuzawa, M., and Kiyokawa, N. (2015). Consistent in-frame internal tandem duplications of BCOR characterize clear cell sarcoma of the kidney. Nat. Genet. 47, 861–863.

van Wely, K.H., Meester-Smoor, M.A., Janssen, M.J., Aarnoudse, A.J., Grosveld, G.C., and Zwarthoff, E.C. (2007). The MN1-TEL myeloid leukemia-associated fusion protein has a dominant-negative effect on RAR-RXR-mediated transcription. Oncogene 26, 5733–5740.

Venneti, S., Garimella, M.T., Sullivan, L.M., Martinez, D., Huse, J.T., Heguy, A., Santi, M., Thompson, C.B., and Judkins, A.R. (2013). Evaluation of histone 3 lysine 27 trimethylation (H3K27me3) and enhancer of Zest 2 (EZH2) in pediatric glial and glioneuronal tumors shows decreased H3K27me3 in H3F3A K27M mutant glioblastomas. Brain Pathol. 23, 558–564.

Wu, G., Broniscer, A., McEachron, T.A., Lu, C., Paugh, B.S., Becksfort, J., Qu, C., Ding, L., Huether, R., Parker, M., et al.; St. Jude Children's Research Hospital–Washington University Pediatric Cancer Genome Project (2012). Somatic histone H3 alterations in pediatric diffuse intrinsic pontine gliomas and non-brainstem glioblastomas. Nat. Genet. 44, 251–253.

Yan, H., Parsons, D.W., Jin, G., McLendon, R., Rasheed, B.A., Yuan, W., Kos, I., Batinic-Haberle, I., Jones, S., Riggins, G.J., et al. (2009). IDH1 and IDH2 mutations in gliomas. N. Engl. J. Med. 360, 765–773.